

SMALL SCALE SURFACE DEFORMATION MONITORING IN MINING REGIONS USING DIFFERENTIAL RADAR INTERFEROMETRY.

Ireneusz Baran and Mike P. Stewart

*Western Australian Centre for Geodesy,
Department of Spatial Sciences, Curtin University of Technology
GPO Box U1987, PERTH WA 6845 Australia*

Abstract

The application of synthetic aperture radar interferometry (InSAR) to deformation monitoring encounters problems due to noise in the interferometric phase measurement, caused by a number of decorrelation factors. These factors dramatically reduce the capabilities of radar interferometry in many applications, and, in particular, compromise detection and analysis of small-scale deformations. A methodology for assessing the ability of InSAR to monitor surface deformation induced by mining activities in terms of the expected achievable accuracy and the minimum recognisable area of deformation, is proposed. This assessment is based on both simulated and real data. Sets of representative deformation models have been created and the associated phase from these models has been introduced to real SAR data acquired by ERS-1/2 satellites. Subsequently, interferograms have been derived and surface deformation has been estimated. In each case, the resultant surface deformation has been analysed by visual inspection and compared with the 'true' surface deformation as defined by the deformation model. A number of cases of surface motion with varying amplitudes, spatial extent and error characteristics have been simulated, and the results presented will provide an indication of the limits of InSAR deformation resolution. Furthermore, the wavelet transform is proposed as a tool for extended analysis of phase interferograms.

1 Introduction

Synthetic aperture radar interferometry is a technique that enables production of Digital Terrain Models (DTM) and detection of surface motion at the centimetre level using radar signals transmitted from satellites. Deformation observations are made possible by the fact that surface motion caused by natural and human activities generates a local phase shift in the resultant interferogram. The magnitude of surface deformation can be estimated directly as a fraction of the wavelength of the transmitted signal. Differential InSAR (DInSAR) eliminates the phase signal due to topography to yield a differential interferogram in which the signature of surface deformation can be seen.

Since the late eighties many applications of radar interferometry have been developed, including: the observation of ground motion over agricultural areas (*e.g.* Gabriel *et al.*, 1989), creating high accuracy digital terrain models (DTM) (*e.g.* Zebker and Goldstein, 1986) and high resolution deformation monitoring of the earth's crust with millimetre accuracy (*e.g.* Strozzi *et al.*, 2000).

First attempts to apply InSAR for mining subsidence monitoring proved the method's viability to measure deformation at the centimetre level (Stow and Wright, 1997). This work showed that, compared to conventional surveying techniques, remotely acquired SAR images have the potential to improve subsidence detection and modelling by increasing the quantity and quality of collected data. However, the balance between adopting a useable temporal baseline (in terms of coherence) and allowing a suitable length of time to lapse for a measurable amount of subsidence to occur needs to be found. Furthermore, it was shown that agriculture land and unfavourable weather conditions considerably decrease the utility of InSAR for deformation monitoring. Perski (1998) also confirmed the usefulness of radar interferometry for environmental monitoring as well as for detecting the dynamics of land subsidence caused by underground mining activities, over the Upper Silesian Coal Basin in Poland. The high accuracy of the InSAR data was demonstrated by its agreement with the ground control points (Perski and Jura, 1999).

Following Massonnet and Feigl (1998), the necessary condition for deformation detection by radar interferometry implies that maximum detectable deformation gradient (MDDG) is one fringe per pixel. In addition, MDDG can be defined by the dimensionless ratio of the wavelength to the pixel size. According to this statement, radar interferometry should be able to detect very small vertical and spatial deformation. Unfortunately radar interferometry suffers from noise in the interferogram phase measurement, which is caused by the decorrelation effects that can be categorized as follows: (i) thermal, (ii) temporal, (iii) geometrical, (iv) Doppler centroid and (v) processing induced decorrelation (Zebker and Villasenor, 1992). In addition, the interferogram contains biases due to satellite orbit errors and atmospheric heterogeneity. Thus, the very small deformation signal can be undetectable if the level of noise is too high. Interferometric phase can be improved by many methods at different processing levels. One of them is filtering of the interferometric phase (e.g. Bo *et al.*, 1999; Goldstein and Werner, 1998). However, while filtering reduces noise in the interferogram, it does not necessarily enhance or recover the signal. Furthermore, the impact of the filter can significantly change the structure of the interferogram.

In this paper, a methodology that can assess the capabilities of radar interferometry as method for small-scale deformation detection is introduced. This method consists of (i) simulation of deformation, (ii) generation of deformation phase values, (iii) insertion of the simulated deformation phase information into a real SLC image, (iv) DInSAR processing, and (v) analysis of the differential interferogram to estimate the signature of the recovered deformation signal, in relation to the original simulated deformation model.

2 Deformation simulation

The most common shape of underground or surface mine deformation on the Earth surface is circular or elliptical sag (e.g. Perski, 1998). To model such deformation the two-dimensional elliptical Gaussian function (eq. 1) has been adopted:

$$f(R, A) = \frac{1}{2\pi\sigma_R\sigma_A} \exp - \left[\frac{(R - \mu_R)^2}{2\sigma_R^2} + \frac{(A - \mu_A)^2}{2\sigma_A^2} \right] \quad (1)$$

where R and A are the coordinates of the model in the range and azimuth directions respectively. Assuming the mean values (μ_R, μ_A) equal 0, by changing the standard deviations components σ_R and σ_A , an elliptical shape for the simulated deformation can be achieved. Furthermore, by scaling the model, a surface deformation gradient can also be simulated. For simplicity, it has been assumed that vertical deformation derived from the model expresses surface subsidence along the direction of satellite line of sight.

Several models, varying in spatial extent (R/A) and the deformation amplitude (h), have been generated (Fig. 1). The spatial minimum extent of the simulated deformation models has been set at 3×25 pixels (single pixel size is $20\text{m} \times 4\text{m}$). Moreover, for each model, the amplitude of the vertical deformation has been increased from 14mm (half of the phase cycle) up until the MDDG is preserved. The simulated models' details are listed in Table 1.

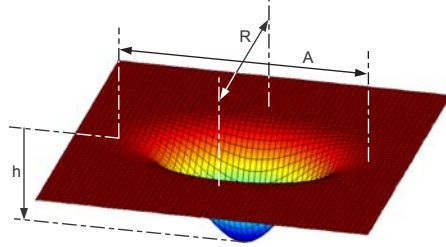


Fig. 1 Simulated deformation model.

By converting the simulated deformation model to their associated phase values ($28\text{mm} = 2\pi$), the change in phase (Φ_{SR}) along the radar line of sight may be computed. The simulated phase is next added as a patch into the phase (Φ_S) of a real radar image (e.g. slave image). The phase (Φ_{SN}) of the new created image is then defined according to Eq. (2)

$$\Phi_{SN} = \Phi_S + \Phi_{SR} \quad (2)$$

If the new phase value (Φ_{SN}) is greater than $\pm\pi$, the phase is wrapped again. Moreover, the amplitude of the original image is not changed ($|a_{SN}| = |a_S|$) (Fig. 2a). The simulated phase patches are added in the areas characterised by different coherence values. This approach of incorporating simulated phase according to deformation model into the real image ensures that the characteristics of the noise in the simulated model are realistic.

Table 1: Deformation models parameters

	Models											
	M1	M2	M3	M4	M5	N1	N2	N3	O1	O2	P1	P2
h [mm]	14	28	56	84	112	14	28	56	14	28	14	28
R/A [m]	480 / 960					280 / 480			140 / 220		60 / 100	

Two radar images acquired by satellites ERS-1 and ERS-2 over the Western Australia Goldfields mining region have been processed. The radar image details are listed in Table 2. The precise orbits for the satellites ERS-1/2 provided by Delft were used (Scharroo and Visser, 1998). To reduce topographical effects, the GEODATA 9 Second Digital Elevation Model Version 2, provided by the Australian Surveying and Land Information Group (AUSLIG), has been used.

Table 2: The used datasets of radar images

Product / Satellite	Orbit	Frame	Acquisition date
SLC / ERS-1	22650	4164	14-Nov-1995
SLC / ERS-2	9991	4164	19-Mar-1997

After the phase of the simulated deformation model has been introduced into the slave image, both images have been processed using the Delft University public domain InSAR software "Doris" (Kampes and Usai, 1999). The interferometric phase difference ($\Delta\Phi$) can be defined as:

$$\Delta\Phi = \Phi_M - (\Phi_S + \Phi_{SR}) + n \quad (3)$$

where n is the sum of noise preserved in both images as well as the noise introduced during the interferometry processing procedure.

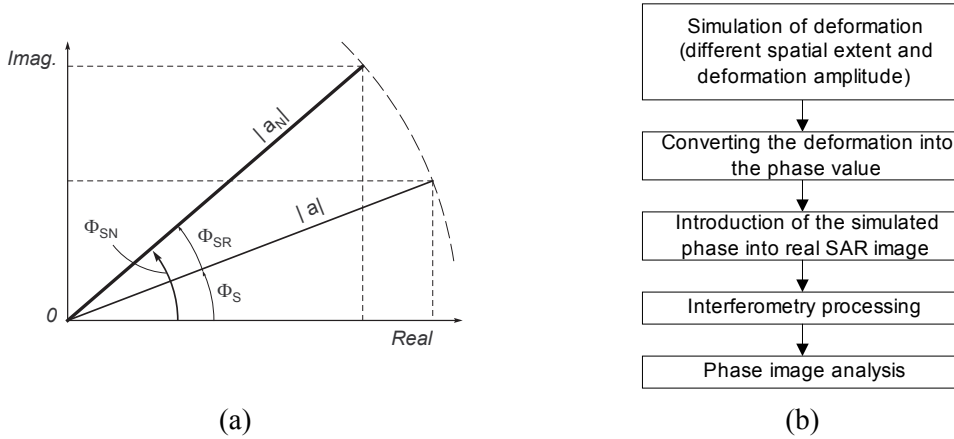


Fig. 2 (a) Definitions of amplitude and phase, and (b) proposed methodology.

If the perpendicular baseline component is sufficiently short, the topography contribution can be neglected and the original phase value (Φ_S) of the slave image and the phase (Φ_M) of the master image should be cancelled during the interferometry process. In practice, it is very difficult to obtain radar images with a very small perpendicular baseline and usually the topography contribution has to be removed from the interferogram in order to obtain the signature of deformation. Therefore, assuming the topography contribution has been subtracted, Eq. (3) can be rewritten as:

$$\Delta\Phi = \Phi_{SR} + n \quad (4)$$

The phase difference ($\Delta\Phi$) in the differential interferogram should contain the phase (Φ_{SR}) component due to the simulated deformation. If the phase (Φ_{SR}) can be revealed on the differential interferogram, it is assumed that the deformation could be observed. Fig. 2b shows the concept of the proposed methodology.

3 Interferometry Analysis Based on Deformation Models

Different deformation models varying in spatial extent and vertical amplitude have been compared visually with their signatures from their respective differential interferograms after interferometry processing. Fig. 3a and Fig. 3b show the interferometric phase of the simulated deformation models M and O (defined in Table 1) and the signature of these models onto the differential interferogram after interferometry processing. The phase due to modelled deformation was added into the slave image in areas characterised by different coherence values ranging from 0.3 to 0.5. The interferogram based on the given radar images (Table 2) is characterised by overall low coherence, due to the long temporal baseline. This factor results in the limited range of coherence values tested. However, the method is also applicable for interferograms with all range of coherence.

It was found that, for constant coherence (rows on the Fig. 3), as the amount of vertical deformation increases, it becomes increasingly difficult to correctly interpret the interferometric phase ($\Delta\Phi$). For instance, for the interferometric phase related to models M1, M2, M3, which represent half, one and two fringes respectively, the number of fringes can be measured correctly. However, for the interferometric phase related to models M4 and M5 (3 and 4 fringes), it was not possible to unequivocally estimate the number of fringes. However, as the magnitude of increasing deformation amplitudes is more difficult to retrieve, the overall

deformation contour pattern is more easily recognised. The extent of the deformation for the ‘M’ family of models could be recognised on the interferogram for coherence values of 0.35 and above, while for models ‘N’ the coherence threshold was determined at the level of 0.40. Furthermore, very small deformation models ‘O’ could be detected at coherence level of 0.50. In addition, the phase of the smallest deformation models ‘P’, were beyond recognition for coherence equal to 0.55 and smaller. In summary, the minimum recognisable deformation extent was found to be for model ‘O’. The spatial extent of this model (140x220 m) and deformation amplitude (0.5 and 1 fringe) could be recognised at the coherence level 0.55.

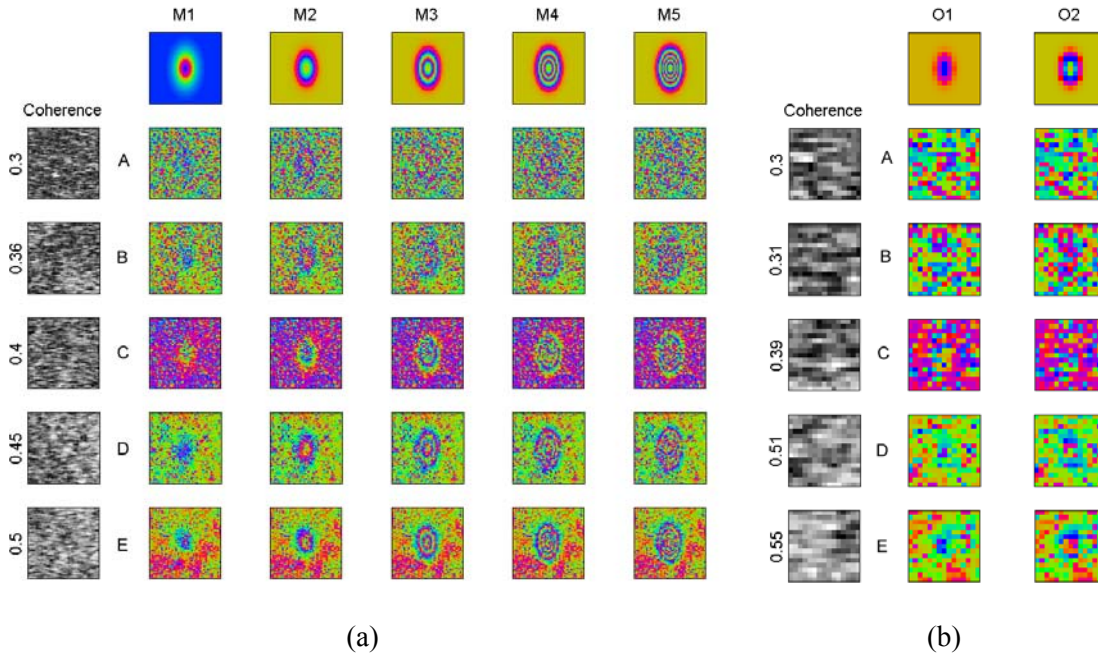


Fig. 3 (a) Interferograms of the simulated models M1 to M5 and (b) O1, O2 as well as their signature after interferometry processing for different coherence area (horizontal rows A to E). No phase filtering was applied.

All the above analyses are based on visual inspection of the differential interferogram. However, the question emerges as to whether the interpretation of the interferometric phase could be extended and additional information revealed. In the next two sections, a preliminary analysis of the simulated differential interferograms using wavelet transforms is presented.

4 Wavelet Transform

The wavelet transform is a relatively new mathematical tool developed in the 1980s by Grossmann and Morlet (1984). Subsequently improved, today it is widely used in many applications, for instance in: image compressing and enhancement, pattern recognitions, geophysics, and any kind of signal analysis. The wavelet is a specially defined wavelike function, for which several conditions must be satisfied (Addison, 2002, p.9). The wavelet transform is capable of describing a highly localised transient signal, making it useful for this analysis as surface deformations caused by mining activities are highly localized in the space domain. Mathematically, the wavelet transform is the process of convolution of a signal with a wavelet kernel. Some wavelet kernels will correlate better with specific signal than others. Therefore, five different 2-D continuous wavelet functions have been chosen: (i) Halo (Dallard and Spedding, 1993), (ii) Perrier (iii) Paul (Perrier *et al.*, 1998), (iv) Poisson and (v) Morlet (Grossmann and Morlet, 1984). These were analysed in order to adopt the most suitable for this

study. Two criteria have been established which the wavelet function should satisfy in order to be used in further analysis:

- The wavelet power spectrum should match the Fourier power spectrum as accurately as possible.
- The overlap between frequency bands determined by the Fourier power spectrum of the wavelet for different ranges of scale should be minimum.

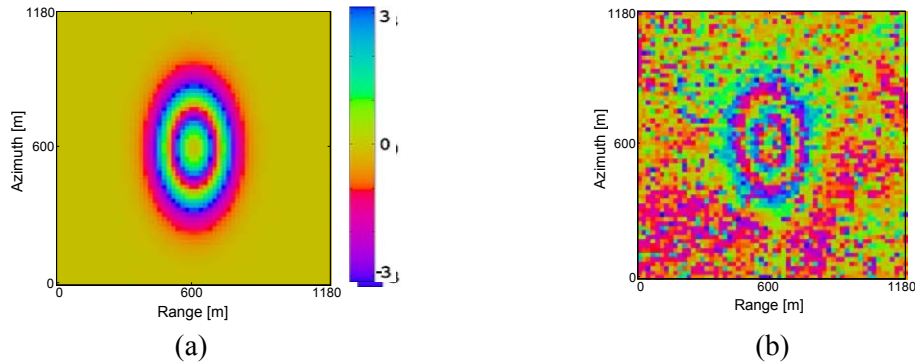


Fig. 4 (a) wrapped phase of the 'M3' deformation model and (b) its interferogram signature ('M3E') (colour bar in radians).

Based on an initial assessment against established criteria, the wavelet Halo was chosen as the most suitable for the extended analysis of the interferometric phase.

5 Results From Wavelet Analysis

In this section the differential interferogram simulations are analysed using the Halo wavelet transform. Fig. 5 shows the analysis of the phase image of the deformation model 'M3' and its interferogram signature 'M3E'. The corresponding scalogram plots reveal the spatial distribution of the wavelet power spectrum. Comparison of the power spectra can provide an indication of the similarities between two signals. It can be seen that the wavelet power spectrum of the 'M3E' interferogram is almost twice as weak as its model 'M3' due to the introduction of noise. However, the same features can be still recognised on both scalograms. At the chosen scale (150m) the wavelet power spectrum shows four spots (numbers 2 and 2') that are associated with the interferometric phase change from the maximum ($+\pi$) to the minimum ($-\pi$) value. Based on this information, the number of fringes can be determined from the scalogram plot even the fringes are noisy. An additional concentration of the energy has been also observed on the scalogram of the 'M3E' (number 4') that could be explained by the long wavelength phase change in the area surrounding the modelled deformation.

From this introductory study, it may be proposed that the application of wavelet analysis to interferometric phase can reveal the valuable information such as: (i) the discontinuities (visible at the vertical cross-sections over the scalogram), and (ii) the different scale components (visible at the horizontal cross-section of the scalogram). In addition, the wavelet transform can be used to reduce the level of noise in the interferogram by filtering out scale components recognised as noise. Whilst this application of wavelet analysis did not reveal any additional information that could directly determine the interferometric phase, it may be used as an additional source of information to support the visual inspection of the analysed interferogram.

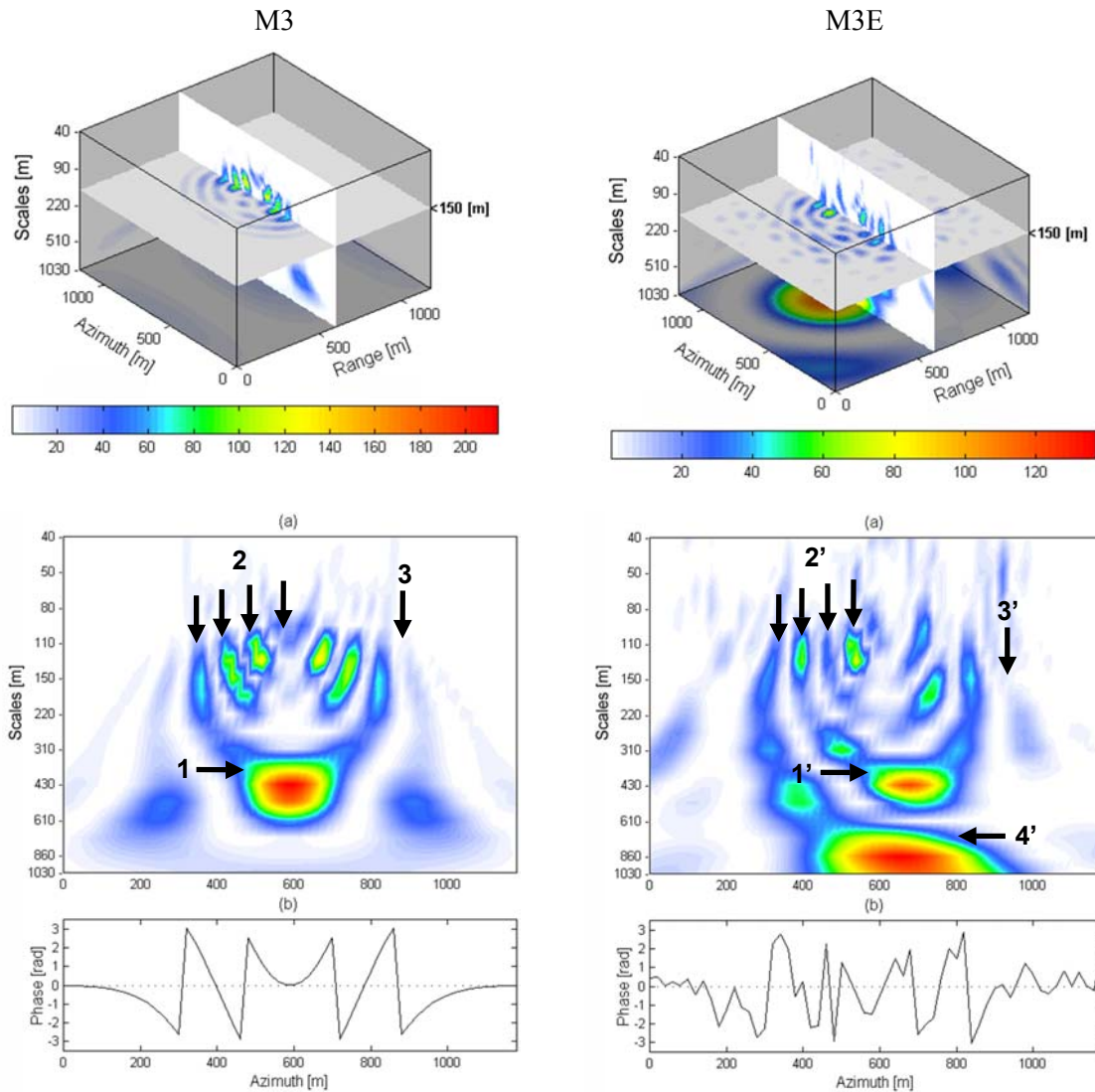


Fig. 5 The left hand side shows the scalogram of the model ‘M3’ for wavelet transform Halo. The horizontal plane shows the wavelet power spectrum for a particular scale (150 m). The vertical axis indicates different scale values, while the horizontal scale bar is the wavelet power spectrum. Figure (a) shows the cross-section over the scalogram in azimuth direction, while figure (b) shows the cross-sections along the corresponding wrapped phase interferogram. Range equals 600 m. The right hand site shows the same figures corresponding to the signature of the model ‘M3’ + noise propagated into the interferogram ‘M3E’.

6 Conclusions and Recommendations

By applying a proposed new methodology, the minimum detectable size of deformation has been found on a test interferogram at the level of 120x220 m and a deformation amplitude up to one fringe. The overall low coherence on the test interferogram was the main constraint, resulting in a somewhat limited range of coherence values tested. However, the method should also be applicable for interferograms with a wide of coherence. In addition, the proposed method can be used as a test to determine whether estimated surface deformation is above or below the simulated threshold for a specific level of coherence.

The results based on the proposed methodology may be used to define a functional model that will help to assess whether deformation is detectible or not by radar interferometry based on its spatial size, deformation amplitude and expected level of coherence. Such a model is currently under development.

Finally, the wavelet transform was proposed as a method of analysing interferometry fringes. The results presented represent a preliminary study and not all aspects of the wavelet transform have been researched. However, wavelet methods appear to be promising for aspects of interferogram analysis and noise. The possible application of wavelet techniques to fringe reconstruction is a suggested area for further research.

Acknowledgements

The authors would like to thank the European Space Agency for supply of SAR data, and the Geoscience Australia for providing the GEODATA 9 Second Digital Elevation Model V.2. Thanks to Dr Jonathan Kirby for valuable discussions, as well as for his wavelets analysis software. The first author is funded by an IPRS scholarship from Curtin University of Technology, Western Australian School of Mines.

References

- Addison, P.S. (2002). *The Illustrated Wavelet Transform Handbook*, Institute of Physics, London, 353 p.
- Bo, G., Dellepiane, S. and G. Beneventano (1999). A locally Adaptive Approach for Interferometric Phase Noise Reduction, *Proceedings of IGARSS 1999*, Hamburg, Germany, June-July, 264-266.
- Dallard, T. and G.R. Spedding (1993). 2-D Wavelet Transforms: Generalisation of the Hardy Space and Application to Experimental Studies, *European Journal of Mechanics B/Fluids*, Vol. 12, No. 1, 107-134.
- Gabriel, A.K., Goldstein R.M. and H.A. Zebker (1989). Mapping Small Elevation Changes Over Large Areas: Differential Radar Interferometry, *Journal of Geophysical Research*, Vol. 94, No. B7, 9183-9191.
- Goldstein, R.M. and C.L. Werner (1998). Radar Interferogram filtering for geophysical applications, *Geophysical Research Letters* Vol. 25, No. 21, 4035-4038.
- Grossmann, A. and J. Morlet (1984). Decomposition of Hardy Functions into Square Integrable Wavelets of Constant Shape, *SIAM J. Math. Anal* Vol. 15, 723-736.
- Kampes, B. and S. Usai (1999). "Doris: the Delft Object-Oriented Radar Interferometric Software", in *Proceedings of 2nd International Symposium on Operationalization of Remote Sensing*, 16-20 August, Enschede, The Netherlands.
- Massonnet, D. and K.L. Feigl (1998). Radar Interferometry and its Application to Changes in the Earth's Surface, *Review of Geophysics* Vol. 36, No. 4, 441-500.
- Perrier, V., Philipovitch, T. and C. Basdevant (1995). Wavelet Spectra Compared to Fourier Spectra, *Journal of Mathematical Physics* Vol. 36, 1506-1519.
- Perski, Z. (1998). The Test of Applicability of Land Subsidence Monitoring by InSAR ERS-1 and ERS-2 in the Coal Mine Damaged Region (Upper Silesia), *International Archives of Photogrammetry and Remote Sensing*, Vol. 32, No. 7, 555-558.
- Perski, Z. and D. Jura (1999). ERSSAR Interferometry for Land Subsidence Detection in Coal Mining Areas *Earth Observation Quarterly* No. 63, 25-29.
- Scharroo, R. and P. Visser (1998). Precise Orbit Determination and Gravity Field Improvement for the ERS Satellites, in *Journal of Geophysical Research*, Vol. 103, No. C4, 8113-8127.
- Stow, R.J. and P. Wright (1997). Mining Subsidence Land Surveying by SAR Interferometry, *Proceedings of the Third ERS Symposium*, Florence, <http://earth.esa.int/florence/papers/stowetal/387c.htm>.
- Strozzi, T., Wegm, U., Werner, Ch. and A. Wiesmann (2000). Measurement of Slow Uniform Surface Displacement with mm/year Accuracy, *Proceedings of IGARSS 2000*, Hawaii, USA, July, 2239-2241.
- Zebker, H.A. and R.M. Goldstein (1986). Topographic Mapping from Interferometric Synthetic Aperture Radar Observations, *Journal of Geoph. Research*, Vol. 91, No. B5, 4993-4999.
- Zebker, H.A. and J. Villasenor (1992). Decorrelation in Interferometric Radar Echoes, *IEEE Transactions on Geoscience and Remote Sensing*, Vol. 30, No. 5, 950-959.